crystals

MDPI

Review

Path Dependency of Plastic Deformation in Crystals: Work Hardening, Crystallographic Rotation and Dislocation Structure Evolution

Zhen-Wei Zhang, Zheng Li, Ying Liu and Jing-Tao Wang *

School of Materials Science and Engineering, Nanjing University of Science and Technology, Nanjing 210094, China; zhangzhenweisamuel@163.com (Z.-W.Z.); lizheng@njust.edu.cn (Z.L.); liuying517@njust.edu.cn (Y.L.)
* Correspondence: jtwang@njust.edu.cn

Abstract: This paper reviewed the research progress of studies on the crystal rotation of single crystals that were deformed by tension and shear and the influences of crystal rotation and dislocation evolution on strain hardening behavior in crystals that were deformed with different initial orientations. The crystal rotation is entirely different depending on whether the single crystal was deformed by tension or shear. A three-stage work hardening behavior, which is not one of the intrinsic properties of materials, is generated when FCC metallic single crystals are deformed by tension along unstable oriFigurFigurentations, but single crystals do not exhibit this three-stage hardening behavior when they are deformed by simple shear at room temperature. Under tension, crystal rotation causes the transition from work hardening stage I to stage II, while the transition from work hardening stage II to III is caused by dislocation evolution. The evolution of the dislocation structure is related to deformation loading and can be classified into three types when a crystal is deformed by tension. Different from tension, shear stress can directly act on one of the 12 slip systems when a crystal is deformed by simple shear. When FCC single crystals are deformed by shear along the $(1\bar{1}1)[110]$, $(111)[11\bar{2}]$ and $(001)[110]$ orientations, the single slip system, co-planar slip systems and co-directional slip systems are activated, respectively, and the crystals hardly rotate under the shear conditions. The slip direction of [110] forces the crystal to rotate toward the shear direction under simple shear. The dislocation tangles tend to form the dislocation cells and wall structures when multiple slip systems are activated under simple shear.

Keywords: single crystal; crystal rotation; work hardening; dislocation evolution; tension; simple shear

Citation: Zhang, Z.-W.; Li, Z.; Liu, Y.; Wang, J.-T. Path Dependency of Plastic Deformation in Crystals: Work Hardening, Crystallographic Rotation and Dislocation Structure Evolution. *Crystals* **2022**, *12*, 999. https://doi.org/10.3390/cryst12070999

Academic Editor: Pavel Lukáč

Received: 21 May 2022
Accepted: 5 July 2022
Published: 19 July 2022

1. Introduction

Single crystals are defined as the molecules or atoms that are contained in a specimen and are regularly and periodically arranged in a three-dimensional space [1], which are usually prepared using the Bridgman technique or the strain annealing technique. Directional cutting based on the Euler angles (as measured by electron backscattering patterns (EBSD) [2–6]) is usually used for the preparation of test pieces. Single crystals have anisotropic and crystallographic symmetry with no grain boundaries and offer advantages in the evaluation the effects of different stress states on the slip activity within a specific slip system. Generally, when a single crystal is deformed by tension, it is accompanied by the formation of deformation bands (DBs), dislocation movement or the activation of double slip systems or multiple slip systems to accommodate any incompatible strains [7]. When polycrystalline metals deform plastically, the dislocations tend to pile up in the grain boundaries, which influence the work hardening behavior of the metals. In addition, studies on the crystal rotation of polycrystalline grains are much more complicated because multiple slip systems are activated when the deformation propagates into the adjacent grains [8–10].

The grains in polycrystalline materials rotate toward several preferred orientations after tensile deformation. As a result, investigations into the strain hardening of single crystals with specific initial orientations can make the activation of deformation mechanisms predictable and controllable and explain the preferred orientations of polycrystalline materials after plastic deformation [11].

Work hardening occurs when metallic single crystals are deformed by tension, which was firstly proposed by Diehl [12]. The three-stage work hardening behavior of single crystals usually occurs during tensile deformation and comprises the easy glide stage (work hardening stage I), linear hardening stage (work hardening stage II) and parabolic stage (work hardening stage III) [13,14]. Work hardening research is the most difficult remaining problem in classical physics and no unanimous conclusions have been drawn until now [15–18].

Single crystal specimens are put into a framework using top and bottom fixtures under tension. On either side of the deformation zone, the crystals cannot glide freely without constraint, so the crystals rotate, thereby forcing the slip direction to rotate toward the direction of the tensile axis. The crystal rotation of single crystals under tension, compression or shear can be observed from the pole figures in the EBSD by comparing the as-deformed orientations to the known orientations in the undeformed state, while the actual orientations of single crystals under specific strain can be illustrated using stereographic projection [19–22]. The crystal rotation of metallic single crystals during plastic deformation is a repeated iteration process, which is caused by the repetitively change in orientation factor and further results in geometric hardening or softening [23]. The crystal rotation of a single crystal under tension induces an increase in dislocation density. The increasing rate in dislocation density is sensitive to the work hardening rate during tensile deformation. To observe crystal orientation and dislocation density in real time and to avoid dislocations gliding out of the sample surface, the in situ observation of a microtest to record the crystal orientation during plastic deformation is necessary [24,25], which can be realized by in situ TEM [26], in situ XRD [27] or in situ EBSD [28].

Simple shear deformation can be characterized as the external stresses that act on a sample being staggered for a short distance, making the material on both sides of the shear plane generate relative gilding. Although shear (at an angle of 45° to the tensile axis) can, for example, be realized by stretching, the constraints from the external actions on the testing sample are very different, i.e., the constraints from axial symmetry under tension vs. twofold symmetry under simple shear, where the sample has more freedom for deformation under tension than under simple shear. As the Schmid factor ranges from 0 to 1, externally applied shear stress has the possibility of being parallel to the slip plane and slip direction, which can eliminate the effects of normal stress [29,30] and a single slip system is thus forced to be activated. Crystal rotation behaviors are much more complicated when FCC metallic single crystals are deformed by simple shear [31,32] and the crystal rotation mechanism of single crystals under simple shear is still not clear and needs to be further investigated. The shear plane and shear direction rotate toward a stable orientation when the crystal is deformed by simple shear. A complete work hardening theory could be established by investigating the effects of crystal rotation and dislocation evolution on the work hardening behaviors of single crystals that were deformed by simple shear. This paper briefly reviewed the research on the path dependency of plastic deformation in crystals from the viewpoints of work hardening, crystallographic rotation and dislocation structure evolution.

2. The Research Progress of Studies on Metallic Single Crystals under Tension

2.1. The Effects of the Crystal Rotation of Metallic Single Crystals on Strain Hardening

Work hardening depends on the crystalline structure of a metal and FCC metals, such as aluminum and copper, typically show stronger hardening than BCC metals, such as iron and tungsten [33]. After tensile deformation, the flow stress obviously depends on the

dislocation density and the relationship between the axial stress σ and dislocation density ρ is shown below:

$$\sigma = \sigma_0 + \alpha\mu b\rho^{1/2} \quad (1)$$

where μ is the shear modulus, b is the dislocation strength and α is a coefficient.

The engineering stress and strain curve $\sigma - \varepsilon$ can be obtained after tensile deformation, while the true stress and true strain curve $\sigma_T - \varepsilon_T$ can be calculated as below during the uniform deformation stage:

$$\sigma_T = \sigma(1+\varepsilon) \quad (2)$$

$$\varepsilon_T = \ln(1+\varepsilon) \quad (3)$$

The shear stress τ and shear strain γ of a single crystal under tension can also be calculated when the angles between the slip direction and the slip plane normal to tensile axis (λ_0 and ϕ_0), are known. Then, the $\sigma_T - \varepsilon_T$ curve can be transformed into a $\tau - \gamma$ curve:

$$\gamma = \frac{1}{\cos\phi_0}\left[\sqrt{\exp(2\varepsilon_T) - \sin^2\lambda_0} - \cos\lambda_0\right] \quad (4)$$

$$\tau = \varepsilon\sigma_T \exp(-2\varepsilon_T)\cos\phi_0\sqrt{\exp(2\varepsilon_T) - \sin^2\lambda_0} \quad (5)$$

The stress–strain curve of a single crystal that was deformed by tension can be divided into three distinct stages: the easy glide stage, linear strain hardening stage and parabolic hardening stage [34]. The work hardening behavior of a single crystal strongly depends on the initial tensile orientation of the single crystal as not all of the orientations of single crystals show the three-stage hardening behavior. It is important to refer to the crystallographic rotation under tension, as elucidated by Schmid [35,36]. There are two origins for the hardening of crystals during deformation: the physical hardening caused by the increase in dislocation density and the geometric hardening caused by crystal rotation. As illustrated in Figure 1, single crystal nickel with a [001] orientation exhibited a strong linear hardening, while single crystal nickel with a [111] orientation exhibited a stress drop after an upper yield joint [37]. Only two distinct stages could be observed because multiple slip systems were activated at the start of the deformation, despite the two loading cases responding entirely differently. The low work hardening rate of the [111]-orientated sample was caused by the cross-slip of dislocations to release the dislocation tangles and the accumulation of dislocations to increase the density was diminished.

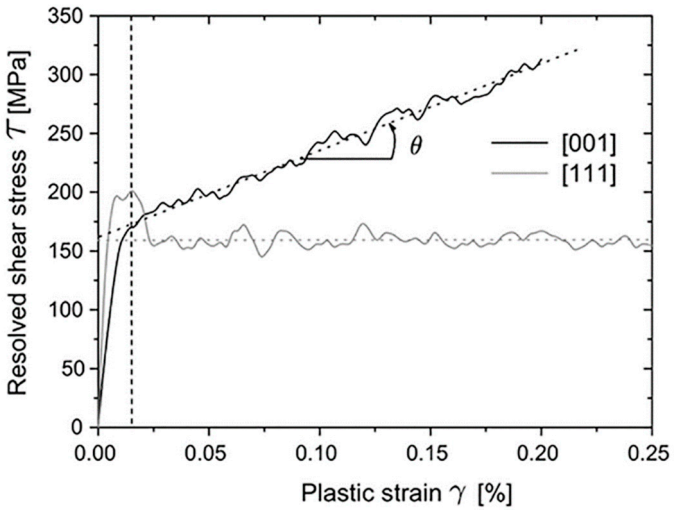

Figure 1. The stress–strain curves of single crystal nickel with an initial orientation of [001] (black line) and [111] (gray line), as obtained by the MD simulations [37].

The initial crystal orientation has a significant effect on the initial slip activation, crystal rotation and dislocation evolution during plastic deformation [38–43]. Recently, Luis et al. [22] reported that the notorious staged hardening of metals as an inflected phenomenon is directly caused by crystal rotation under uniaxial strain and that the mechanisms of dislocation behavior are the same across all stages of metal hardening. This conclusion was based on the atomistic simulations of single crystal aluminum with [001], [111], [112], [101], [102] and [213] orientations under uniaxial tension. The corresponding stress–strain curves are illustrated in Figure 2. Leaving aside the quantitative differences between the magnitudes of flow stress in Figure 2a,b, the simulated and experimental stress–strain curves are in remarkable qualitative agreement. The occurrence of crystal rotation under tension with different initial orientations causes characteristic variations in the shapes of the stress–strain curves. The qualitative characteristics of the strain hardening that was observed in the MD simulations are shown in Table 1. The crystals with an initial orientation of [001], [111] and [112] did not rotate during tensile deformation, instead exhibiting simple parabolic stress rise hardening, retaining their initial symmetries and showing no stage hardening, while the other four curves exhibited distinct inflection. The crystals with an initial orientation of [101], [102], [213] and [8 5 13] rotated toward [112], while the crystals with an initial orientation of [212] rotated toward [111].

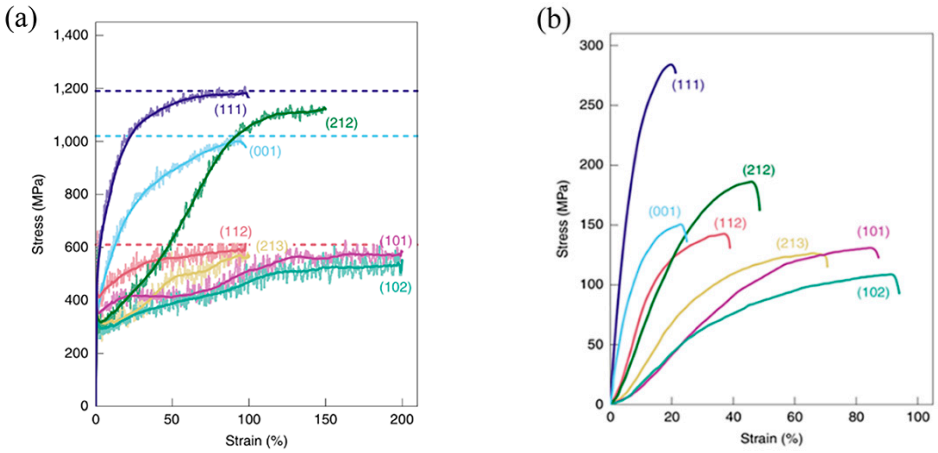

Figure 2. (**a**) The stress–strain curves of single crystal aluminum with initial orientations of [001], [111], [112], [101], [102] and [213], as obtained by the MD simulations [23]; (**b**) the corresponding experimental stress–strain curves, as obtained from tensile straining tests using single crystal copper [14].

Table 1. The qualitative characteristics of strain hardening that were observed in the MD simulations [22].

Initial Axis	Initial Slip Symmetry	Does the Crystal Rotate?	Hardening Response	End Axis
[001]	Eightfold; holds	No	Parabolic	[001]
[111]	Sixfold; holds	No	Parabolic	[111]
[101]	Fourfold; breaks	Yes	Three-stage	[112]
[112]	Twofold; holds	No	Parabolic	[112]
[212]	Twofold; holds	Yes	Three-stage	[111]
[102]	Twofold; breaks	Yes	Three-stage	[112]
[213]	No symmetry	Yes	Three-stage	[112]
[8 5 13]	No symmetry	Yes	Three-stage	[112]

Saai et al. [43] performed tensile experiments using single crystal aluminum with a special initial orientation of [$\bar{1}$25] to investigate crystal rotation during uniaxial tensile deformation. The deformation path is described by the stereographic projection map in Figure 3. At work hardening stage I, dislocations began to glide on the slip system of

(111)[$\bar{1}$01]. As the deformation proceeded to work hardening stage II, the slip direction [$\bar{1}$01] of the crystal rotated toward the tensile axis and continued to rotate toward the [001]–[$\bar{1}$11] symmetry boundary of the stereographic triangle. At this symmetry boundary, the primary slip system of (111)[$\bar{1}$01] and the conjugate slip system of ($\bar{1}\bar{1}$1)[001] were equally oriented for slip and became activated. As it deformed further, the tensile axis rotated along the symmetry boundary toward the [$\bar{1}$12] orientation. However, the axis trajectory slightly overshot the edge and returned to it until the crystal rotated to a stable orientation of [$\bar{1}$12], which indicated that the shear stress that was required for slipping in the conjugate system was higher than that for slipping in the active system.

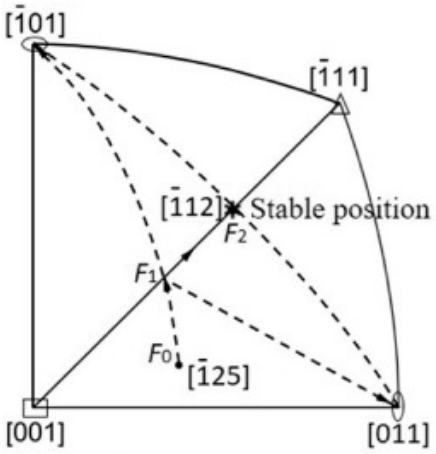

Figure 3. The theoretical rotation behavior of an FCC single crystal specimen under uniaxial tension [27]. The tensile axis starts from F_0, rotates to F_1 following the pathway of $F_0 \rightarrow F_1 \rightarrow [\bar{1}01]$ and then turns to $[\bar{1}12]$ along the edge of the orientation triangle.

Single crystals exhibit significant three-stage hardening characteristics when deformed with unstable initial orientations (such as [212], [213], [101] and [102]) [44]. The transition between work hardening stage I (single slip system) and work hardening stage II (multiple slip systems) is mainly caused by crystal rotation, which causes the breakage of the initially activated mode of slip. Crystal rotation causes the Schmid factor of conjugate slip systems to increase and gradually activate to interact with the primary slip systems to form dislocation tangles, which cause an increase in the work hardening rate and has a significant effect on the motion and evolution of the dislocation. The reorientation of the crystal lattice through the rotation of the tensile axis enables further strain accommodation, which is caused by gliding in the secondary slip system. Crystal rotation may even cause recrystallization under tension and is responsible for the formation of new grains [45]. As the orientation of single crystals is stable at [112], the Schmid factors of the primary slip system and the conjugate slip system are the same, making the flow stresses and dislocation densities approach their asymptotic values [46]. However, it is desirable to note that crystals with an initial orientation of [212] rotate toward the [111] orientation when deformed by tension, as shown in Table 1.

Xu et al. [47] also performed experiments on the uniaxial tensile deformation of [100]- and [110]-oriented single crystal nickel and found that the single crystal nickel with the [110] orientation showed lower yield stress, higher elongation and more complex deformation behavior than the sample with the [100] orientation. There was little crystal rotation when the single crystal nickel was stretched along the [100] orientation and reached [100 12 0] after 35% elongation. This indicated that although multiple slip systems were active simultaneously when the single crystal nickel was deformed along the [100] orientation, there was a slight preference for some slip systems. However, a significant crystal rotation could be observed when the [110]-oriented single crystal nickel was deformed by tension, as shown in Figure 4. It was found that the [110]-oriented single crystal nickel initially performed a single slip along the [10$\bar{1}$] direction on the (11$\bar{1}$) slip plane. The identity of

the slip systems could be verified by comparing the EBSD map and the pole figures. As it deformed further, the single crystal nickel rotated toward the new direction of [20 $\overline{19}$ 0] when a different slip system became activated at a later stage, with a unique slip system $(1\bar{1}1)[10\bar{1}]$ becoming slightly more favored than the other symmetrical slip system. The inverse pole figure shows the crystal orientation after the fracture, as shown in Figure 4b. As the single crystals rotated during tensile deformation, the initial deformation mode was broken. The (111) planes rotated 30°–32° from their initial orientations and the conjugate slip was slightly more favored than the other symmetrical slip system. To conclude, the changes in the deformation path of single crystal nickel were caused by crystal rotation and the crystal rotation effect could not be neglected [48].

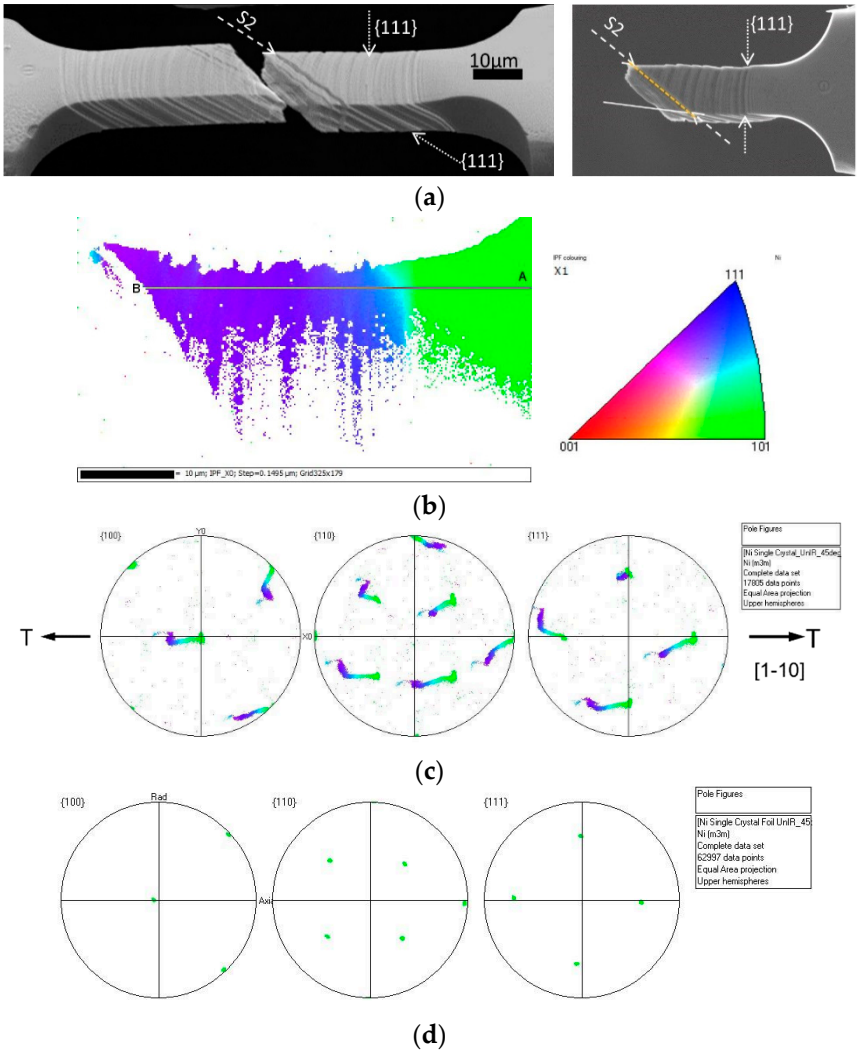

Figure 4. (**a**) An SEM image of the [110]-orientated single crystal nickel after tensile deformation; (**b**) an EBSD inverse pole figure map of the right half of the fractured sample in (**a**,**c**) for the pole figures of single crystal nickel after tensile deformation; (**d**) the pole figures of the [110]-oriented sample before testing [47].

2.2. The Effects of Dislocation Evolution on Strain Hardening under Tension

The dislocations that are generated under tension or compression have a relationship with work hardening behavior and single crystals with different orientations have significantly different dislocation structures [49–54]. As investigated by Mishra et al. [55], the hardening behavior of a metallic single crystal is controlled by dislocation interactions that lead to dislocation junction formation (sessile junctions and glissile junctions) and tangled

dislocation structures. The cross-slip of a single crystal can be induced by temporally higher resolved stress and facilitates the release of tangled dislocation structures.

The work hardening behavior of single crystals that were deformed by tension is directly induced by the increase in dislocation density by means of interactions between parallel dislocations or interactions between forest dislocations [56,57]. The dislocation structures that are formed at different stages of work hardening can be classified into different types according to the initial orientation of the single crystal [58–61]. As crystal rotation is more of a concern for researchers, they have found that the dislocation interaction mechanism is usually caused by crystal rotation due to changes in the Schmid factors of the slip systems, which cause the activation of conjugate slip systems and the three-stage work hardening behavior of single crystals.

Dislocations exhibit dislocation cells or cell block structures when tensile deformation enters work hardening stage III. Dislocation microstructures at higher strains in work hardening stage III could be classified into three types, as shown in Figure 5 [62]. The first type was a cell block structure with straight and parallel sets of cell block boundaries that were aligned with the {111} planes. The dislocation boundary deviated from the slip plane within 10°, where the grains were mostly located in the middle part of the triangle, and finally rotated toward the [112] orientation. Geometrically necessary boundaries (GNBs) were observed in the microstructure, which were straight and parallel and had a well-defined macroscopic orientation with respect to the tensile axis. The second type of microstructure was an equiaxed dislocation cell without GNBs. The grains that demonstrated this type of structure were near the [100] pole. Finally, the grains which were elongated close to the [111] orientation formed the third type of dislocation structure. These dislocations exhibited a cell block structure that deviated from the {111} planes by more than 10°, as shown in Figure 5d. The dislocation boundaries contained short and long segments, but most of them were aligned with the deformation direction. Even when the crystal hardly rotated during tensile deformation, the formation of the dislocation boundaries also caused low-angle misorientation. The low-angle misorientation was caused by crystal rotation when the critical stress exceeded that of the other slip system. This investigation on the dislocation microstructures of an aluminum alloy with a preferred orientation could be used to predict the dislocation structures of single crystals with the orientations of [100], [111] and [112]. To conclude, dislocations that glided in different slip classes could form different dislocation microstructures.

As tensile deformation progresses to multiple glide stage II, dislocation tangles and stable junctions are generated by the transformation of dislocations from one cross-slip system or two glissile junction slip systems to another [44]. Dislocation pinning points are formed at stage II, which are regarded as barriers to dislocation glide. Dislocations from primary and conjugate slip systems become piled up and align to form dipolar walls, which accelerate the increase in dislocation density and have a tendency to form dislocation cells and walls [63,64], thereby causing an increase in the work hardening rate. As moveable dislocations are continuously obstructed by immobile dislocations, when the number of entangled dislocations reaches a certain extent, they may cross-slip to other slip planes and the work hardening transforms into stage III. The most prominent feature of dislocation structures in single crystals at stage III is the formation of cell structures that are parallel to the primary slip plane. The slip bands can be observed during work hardening stage III when dislocations with cellular networks have formed. The misorientation of dislocation cells is small and dislocations with cellular structures are gradually transformed into subgrains. At work hardening stage III, a large number of screw dislocations cross-slip to other slip planes when they encounter obstacles. The work hardening rate decreases and the stress–strain curve exhibits parabolic characteristics in work hardening stage III because entangled dislocations and forest dislocations are released by the cross-slip of dislocations. Considering the effects of crystal rotation on the transition from work hardening stage II to stage III, single crystal aluminum with an initial orientation of [$\bar{1}$25] was deformed by tension. The crystal orientation almost remained stable, which was near [$\bar{1}$12], when the

single crystal aluminum was deformed during the transition from work hardening stage II to stage III. The two original activated slip systems of $(11\bar{1})[011]$ and $(111)[10\bar{1}]$ were maintained in work hardening stage III, even when the crystal rotated in the direction of $[\bar{1}12]$. The effects of crystal rotation on the transition from work hardening stage II to stage III were insignificant due to the slip mode remaining stable with despite the crystal rotation during work hardening stage III. Additionally, the crystal orientation in work hardening stage II rotated to $[\bar{1}13]$ and almost remained stable when it entered work hardening stage III. Thus, the transition from work hardening stage II to stage III was not caused by crystal rotation, but instead by dislocation evolution. The dislocation cells gradually achieved a stable equilibrium in work hardening stage III.

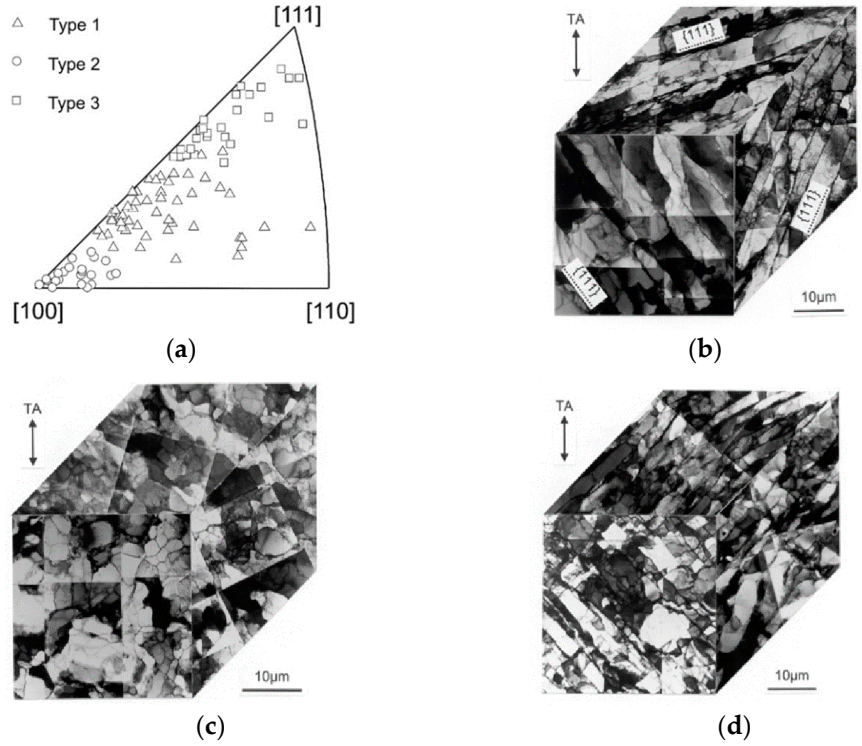

Figure 5. The dislocation structures of a 99.99% aluminum alloy that was deformed by tension: (**a**) the TA orientations of 100 of the grains examined; (**b**–**d**) the TEM diagrams of grains with type I, II and III structures, respectively [62].

Nowadays, the in situ transmission electron microscopy (TEM) technique can observe dislocation movements during tensile deformation in real time and genuinely reflect the dislocation interactions, which helps to make correlations between the dislocation behavior and the work hardening rate [61]. Landau et al. [65] investigated the work hardening behavior of single crystal aluminum that was induced by dislocation dynamic evolution using in situ TEM. When the sample was pre-strained to 10% in the $[\bar{1}\bar{2}2]$ direction, two slip systems were activated and the deformation entered work hardening stage II at the very beginning of tensile deformation. The work hardening rate increased because dislocations with Burgers vectors of $\frac{1}{2}[110]$ and $\frac{1}{2}[10\bar{1}]$ were interacting with each other and dislocation barriers, such as dislocation loops, became obstacles to the movement of gliding dislocations. A tangled dislocation boundary was formed because of the dislocations that bowed out in the $[\bar{2}\bar{1}1]$ trace direction. The evolution of a dislocation boundary at work hardening stage III is illustrated in Figure 6. The cross-slip of dislocations that was generated in work hardening stage III can be observed by the arrows in Figure 6a. The activation of the two slip systems that were characterized as $\frac{1}{2}[110]$ and $\frac{1}{2}[10\bar{1}]$ is also noticeable. The dislocation boundaries were formed due to the cross-slip of dislocations, which could have been generated in work hardening stage II. The effects of the cross-slip of dislocations became more intense

when entering work hardening stage III, causing the number of immovable dislocations to decrease and being responsible for the formation of typical dislocation patterns. The accumulation of dislocations within the cell boundary during work hardening stage III and the dislocation density remained statistically constant throughout work hardening stage III owing to the continuous exhaustion of mobile dislocations at the surfaces. As a result, the work hardening rate decreased during work hardening stage III.

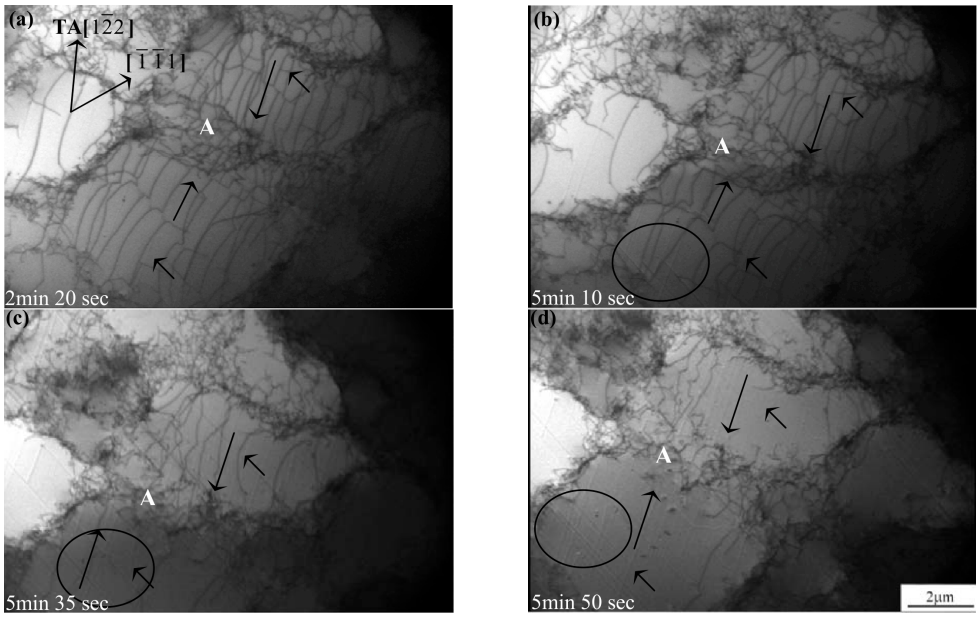

Figure 6. The in situ TEM observations of dislocation boundary evolution and the cross-slip of dislocation when single crystal aluminum was deformed to work hardening stage III [65], (**a**–**d**) frames at the time of 2 min 20 s, 5min 10 s, 5 min 35 s and 5 min 50 s, showing the depletion of the cell's volume from dislocations into the cell's boundary by cross slip of dislocation, respectively.

3. The Work Hardening Mechanism of Single Crystals That were Deformed by Shear

3.1. Different Methods for Shear

Shear deformation takes place when an external force is applied parallel to a point of application on the object while the opposite force is staggered to act on another point of application on the object. When a single crystal is deformed by shear, the geometric shape of the single crystal does not change until the shear stress reaches a particular value. The Schmid factors of FCC single crystals range from 0~1 and is calculated using Equation (6), while the Schmid factors of FCC single crystals under tension only ranges from 0~0.5

$$m = \cos\theta\cos\beta \tag{6}$$

While θ is the angle between the external stress and the slip direction, β is angle between the shear plane normal and the slip plane normal. The dislocation density increases as shear deformation starts and leads to the well-known relationship between shear stress (τ) and dislocation density (ρ) [66]:

$$\tau = \alpha\mu b\sqrt{\rho} \tag{7}$$

where μ is the elastic shear modulus and b is the Burgers vector.

Shear deformation, which is usually referred to simple shear, is a plane strain deformation mode that is characterized by early localization and intensive straining along with shear bands. The schematics of a double shear test are shown in Figure 7a. It can be observed that the specimen had two symmetrically sheared zones and was acted on by an

axial load. The symmetry of the specimen facilitated shear loading and the specimen did not suffer from a change in slip geometry during testing.

Simple shear deformation is developed by constrained shear inside a narrow area. The first simple shear equipment was designed by Miyauchi [67] and later, a simple shear device was developed by Rauch and G'Sell [68,69] using a specially constructed apparatus in which the applied shear stress could act in different crystallographic planes and different crystallographic directions. Nowadays, a double-notched shear specimen in compression mode is used most commonly (which is shown in Figure 7b), probably because the symmetry of the specimen can facilitate shear loading [70–73]. For this technique, the specimens have notches that extend from the opposite surfaces to the middle of the specimens and the interlaminar shear strength of the materials can be measured by double shear. There is an obvious shear region on both sides of the samples and the samples can be sheared by a large shear strain, but the shear strain has a maximum value. Single crystals can shear along a specific shear plane and shear direction and the shear strain is more controllable when FCC metallic single crystals are deformed by simple shear in the shape of a double-notch. The shear deformation zones are localized in the center of the specimens, while crystal rotation and dislocation evolution under simple shear can be observed in the shear zones. This geometry of specimen can make the known slip system in a single crystal activate during shear deformation, which invariably favors the operation of the easy-to-activate basal slip system during shear experiments. However, a sample with a double-notch geometry that is sheared under tension is the most ideal shear mode for single crystals as the specimens can be subjected to larger shear strains, as shown in Figure 7c. In addition, the geometry of an inclined double-notch shear specimen is illustrated in Figure 7d. Appropriately tilted but sharper notches generally seem to result in the most uniform stress fields.

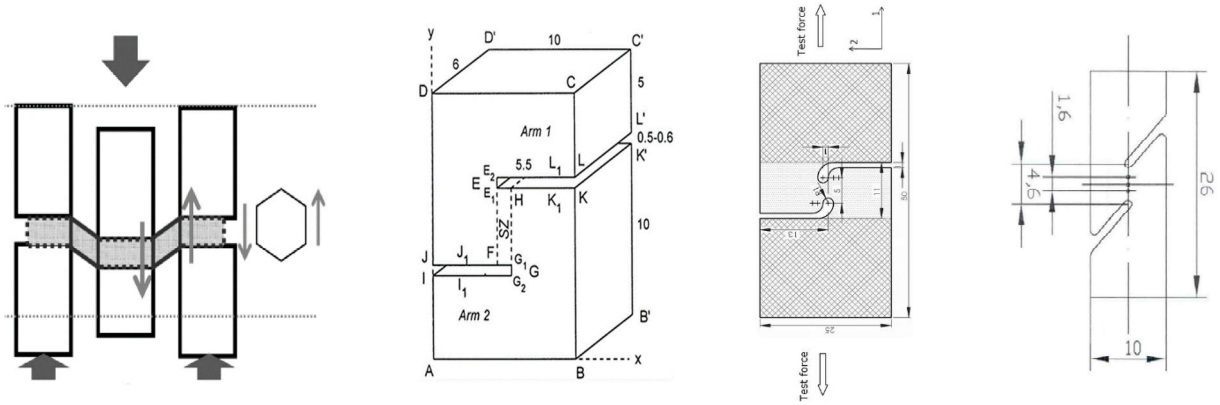

(**a**) (**b**) (**c**) (**d**)

Figure 7. The different ways to directly apply simple shear that have been proposed in the literature: (**a**) a specimen with a double shear zone [74]; (**b**) a double-notch specimen in compression mode [70,71] (SZ is the zone of shear); (**c**) a double-notch tensile–shear specimen [75]; (**d**) a tilted double-notch tensile–shear specimen [76,77].

Other simple shear deformations, such as equal channel angular pressing (ECAP) [78,79], high-pressure torsion (HPT) [80,81] and rolling deformation [82,83], can cause the formation of grain boundaries and significantly refine the grain size.

The three-stage hardening is a kinematic consequence of the co-axiality constraint that is imposed on specimens during standard uniaxial tests [22]. The use of simple shear avoids the specimen suffering from uniaxial deformation, which is only induced by plane constraints in the shear zones. Therefore, metallic single crystals may not show three-stage hardening behavior under simple shear.

The hardening rate depends on the detailed crystallographic configurations of the active systems for a given number of slip systems [84]. As single crystals are sheared along different shear planes and shear directions, specific slip systems are activated, which may

have an influence on the crystal rotation and dislocation evolution mechanisms. The typical dislocation microstructures that are induced by specific slip modes can be observed using TEM because the specific slip modes can be maintained under large shear strains during shear deformation. However, the dislocation microstructures that are formed by single slips, co-planar slips or co-directional slips cannot be maintained under large strains during tensile deformation due to crystal rotation causing the conjugate slip system to become activated when the deformation has an orientation through the middle of the triangle.

3.2. Research on Metallic Single Crystals under Microshear

Over recent years, microshear testing, which represents a kind of simple shear deformation, has received much more attention and has been studied by many researchers [85–89]. Metallic single crystals are widely used to perform microshear experiments because the initial crystallographic orientations of the specimens are specific and crystals with no grain boundaries have no influence on interactions with adjacent grains. The advantage of using microshear geometry, which can be focused ion beam micromachined, is that the slip trace and crystal orientation of a single crystal can be observed in situ using SEM or EBSD. Deformation is localized within the shear zones that exhibit no differences between the two shear zones because the specimens are deformed in parallel and simultaneously during micro-double shear experiments. The selected slip system is preassigned to undergo shear deformation with specific active slip systems, which enables us to observe the dislocation microstructures that are generated by specific slip modes. The possibility of strain hardening from the interactions between dislocations along different planes can be precluded by only pre-selecting one individual slip system before applying simple shear.

Many microshear deformations can be accommodated by dislocation gliding in the {111}[110] slip system [88]. Some researchers have even chosen a shear stress direction that is parallel to the slip direction and the shear plane that coincides with the slip plane, thereby activating the single slip system [87]. Heyer et al. [88] investigated the microshear deformation of single crystal gold along the shear plane of (111) and the shear direction of $[1\bar{1}0]$. Moderate strain hardening was observed under micro-double shear in the $(111)[1\bar{1}0]$ direction with the formation of a few shear bands. It is unlikely that the moderate strain hardening was associated with the activation of a second crystallographic slip system because the single slip of $(111)[1\bar{1}0]$ was activated under the shear stress, which directly acted on the slip system. Seok et al. [90] performed microshear tests using pure magnesium and the shape of the microshear specimen is shown in Figure 8, which was closely oriented to the basal shear. The load partitioning between the two shear segments led to the subsequent activation of the basal slip while the other slip systems, which were not aligned with the loading axis, were quite difficult to operate. The critical resolved shear stress (CRSS) value could be obtained from the microshear deformations according to the mechanical load–displacement data, which could reflect the true material behavior of the basal slip. However, the uniaxial tensile deformation facilitated deformation along multiple pyramidal slip planes, which exhibited extreme strain hardening behaviors, while significant strain softening could be analyzed from the stress–strain curves. Wieczorek et al. [91] performed in situ SEM microshear experiments using single crystal copper, which was pre-deformed under tension along a [100] loading axis with different amounts of strain (strains of 0%, 6% and 20%). The shear stress direction of the samples was parallel to the slip direction $[0\bar{1}\bar{1}]$ and the shear plane coincided with the slip plane $(1\bar{1}1)$. During the [100] tensile loading, the $(111)[10\bar{1}]$ and $(111)[1\bar{1}0]$ slip systems were activated. However, the dislocation slip was promoted in the $(1\bar{1}1)[0\bar{1}\bar{1}]$ slip system in the subsequent microshear tests. The interactions between the $(111)[10\bar{1}]$ dislocations, which were from the tensile preloading of $(1\bar{1}1)[0\bar{1}\bar{1}]$ that was promoted under microshear, resulted in the formation of Lomer–Cottrell junctions, which are immovable and further become obstacles for dislocation movement, thereby causing the work hardening rate of single crystal copper with a 6% pre-deformation strain to be higher than a sample that was only subjected to microshear deformation. The interactions between the dislocations from the $(111)[10\bar{1}]$ and $(1\bar{1}1)[0\bar{1}\bar{1}]$

slip systems were much stronger when single crystal copper was pre-deformed with a 20% strain under tension and thus, caused the highest work hardening rate among the three samples. Therefore, the work hardening behavior was mainly caused by the dislocation interactions between the initial tensile loading and the subsequent microshear testing.

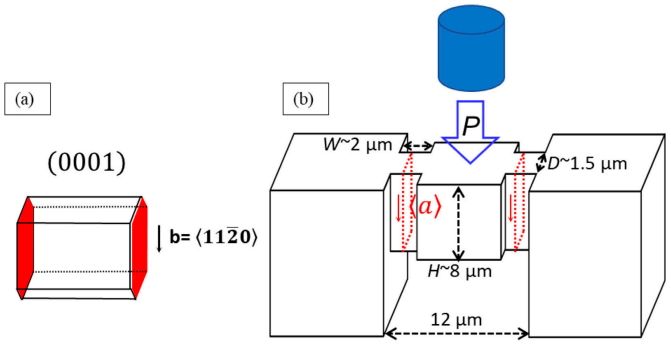

Figure 8. (**a**) A schematic of the shear plane and the shear direction of single crystal magnesium; (**b**) the geometry of single crystal magnesium under microshear [90].

The mechanical anisotropy in single crystals that were deformed by microshear has been studied by Laplanche et al. [89], who investigated the in situ microshear behavior of a single crystal nickel-based superalloy in three different crystallographic shear systems: (111)[01$\bar{1}$], (111)[$\bar{2}$11] and (100)[010]. The corresponding mechanical results are shown in Figure 9. The nickel-based single crystals did not exhibit work hardening stages I and II when they were deformed by microshear, no matter whether they were deformed in the (111)[01$\bar{1}$], (111)[$\bar{2}$11] or (100)[010] direction. The single crystals with a shear plane of (111) were loaded into [01$\bar{1}$] and [$\bar{2}$11] to promote a single slip system (one slip system with a Schmid factor of 1) and double slip systems (two co-planar slip systems with high Schmid factors of 0.87), respectively. The shear system of (100)[010] was chosen in order to make single crystals that were deformed under multiple slip conditions. Localized plastic deformation could be observed during the (111)[01$\bar{1}$] shear loading, while strain localization could still be observed after the (111)[$\bar{2}$11] shear loading. The required shear stress was much higher than that required for tensile deformation in order to initiate sudden deformation events when a single slip system was activated. The mechanical properties of single crystal specimens that were sheared along (100)[010] were similar to those of single crystal specimens that were sheared along [010] under tensile loading and the tendency to localize strain decreased.

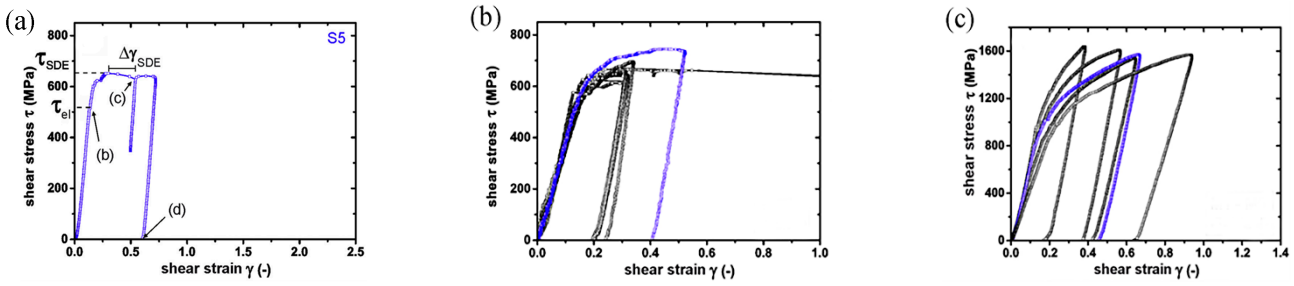

Figure 9. The mechanical results of a specimen (**a**) under (111)[01$\bar{1}$] shear loading (single slip orientation); (**b**) (111)[$\bar{2}$11] shear loading (double slip orientation); (**c**) (100)[010] shear loading (multiple slip orientation) [89].

The yield stresses that were observed in the (100)[010] shear system were in good agreement with [001]-orientated single crystal nickel that was deformed by tensile deformation because the interactions between the different slip systems under multiple slip conditions occurred both during microshear deformation and tensile deformation. However, the shear

stress in the (100)[010] shear system was higher than in the other two shear systems, which can be seen in Figure 9, because the low resolved shear stress acting on the slip systems required much higher external loads to promote plastic deformation.

3.3. Investigations on the Path Dependency of Single Crystals That Were Deformed by Shear

Crystal rotation is much more complicated when single crystals are deformed by simple shear than by tension, even though the crystal rotation mechanism of single crystals that are deformed by tension is already known [92]. However, few researchers have investigated the crystal rotation mechanism of single crystals that are deformed by simple shear because the shear plane and shear stress rotate simultaneously during shear deformations and the stable orientation of the shear plane depends on the initial orientation of the specimen. Crystal rotation is only characterized by the orientation of the tensile axis in the stereographic projection during tensile deformation, while not only the shear direction but also the shear plane needs to be designated in the stereographic projection during shear deformation.

Some studies have used polycrystals to perform simple shear deformation tests and found that a homogeneous and stable grain structure is obtained when the shear strain is large enough and that the crystal orientation is stable at $(1\bar{1}1)[110]$, $(111)[11\bar{2}]$, (001)[110] and $(1\bar{1}2)[110]$ [93,94]. The Schmid factors of the twelve slip systems in these four shear plane and direction situations ($(111)[11\bar{2}]$, $(1\bar{1}1)[110]$, (001)[110] and $(1\bar{1}2)[110]$) were calculated and are presented in Table 2. A single slip is activated for crystals that were sheared along $(1\bar{1}1)[110]$ or $(1\bar{1}2)[110]$, which could eliminate the possibility of strain hardening being caused by interactions between dislocations from different slip planes. The crystals hardly rotate along the shear plane of $(\bar{1}11)$ and shear direction of [110] because the Schmid factor of the $(1\bar{1}1)[110]$ system is close to 1, which causes dislocation gliding in the steady state. The co-planar slip systems are activated when metallic single crystals are sheared along $(111)[11\bar{2}]$. The crystal orientation remains stable due to the $(111)[10\bar{1}]$ and $(111)[01\bar{1}]$ slip systems having the same Schmid factor of 0.866. The shear direction is the equivalent direction of the two activated co-planar slip systems, so the crystals hardly rotate when single crystals are sheared along $(111)[11\bar{2}]$.

Table 2. The Schmid factors for four shear planes and directions.

Slip Systems	Shear Directions and Planes			
	$(111)[11\bar{2}]$	**$(1\bar{1}1)[110]$**	**(001)[110]**	**$(1\bar{1}2)[110]$**
$(111)[1\bar{1}0]$	0	0	0	0
$(111)[10\bar{1}]$	0.866	0.167	0.289	0.236
$(111)[01\bar{1}]$	0.866	0.167	0.289	0.236
$(\bar{1}11)[110]$	0.192	0.333	0.577	0
$(\bar{1}11)[101]$	0.096	0.167	0.289	0
$(\bar{1}11)[01\bar{1}]$	0.324	0.167	0.289	0
$(1\bar{1}1)[110]$	0.192	1	0.577	0.942
$(1\bar{1}1)[10\bar{1}]$	0.324	0.5	0.289	0.471
$(1\bar{1}1)[011]$	0.096	0.5	0.289	0.471
$(11\bar{1})[1\bar{1}0]$	0	0	0	0
$(11\bar{1})[101]$	0.096	0.167	0.289	0.236
$(11\bar{1})[011]$	0.096	0.167	0.289	0.236

Moreover, the co-directional slip systems were activated when single crystals were deformed by shear along (001)[110], as shown in Table 2. As co-directional slip systems are activated during shear deformation, such as rolling, the cross-slips are dominant during

simple shear and a boundary plane is formed. Dislocations are trapped at the boundary plane and they either annihilate each other or form dipoles and become obstacles that hinder the movement of gliding dislocations, which promote the work hardening rate. Liu et al. [95] investigated the dislocation boundary formation of single crystal aluminum that was deformed by cold rolling. Their results showed that rotations could be readily produced by a shear amplitude imbalance between the two pairs of critical co-directional slip systems. The boundaries were likely formed in the co-directional slip systems because the dislocations could easily cross-slip to another slip plane and the boundaries could have originated from co-directional slip systems that were activated during shear deformation. As a result, the work hardening rate was relatively low when the co-directional slip system was activated.

The shear zones are constrained by both sides of a specimen, so simple shear deformation is a constrained deformation. The orientation of the normal direction of a double-notched specimen is relatively stable due to the constraints of the deformation, while the shear stress forces cause the crystals to rotate toward the soft orientation and the shear direction tends to rotate toward the slip direction of [110]. Takayama [96] investigated the texture evolution in an aluminum and 3% magnesium alloy and the (110) pole figure revealed that a texture component of <110> was parallel to the slip direction, which indicated that the shear direction was rotating toward the slip direction. The grain rotation in the local areas promoted the rotation of the {111} slip plane toward the shear plane and the rotation of the [110] slip direction toward the shear direction. In addition, Zhang [31] investigated single slip system polycrystalline models of ice crystals and found that the slip planes could rotate both toward and away from the shear plane. As FCC metallic single crystals have 12 slip systems, it can be deduced that the shear direction rotates toward the slip direction of <110>. The crystal orientation remains stable when sheared along (001)[110], (110)[1$\bar{1}$0] and (111) [1$\bar{1}$0].

3.4. The Effects of Dislocation Evolution on the Work Hardening of a Single Crystal That Was Deformed by Shear

When a single crystal is deformed by shear, dislocations are generated to accommodate the applied stress–strain conditions. The work hardening behavior is anisotropic when single crystals are deformed by simple shear along different shear directions and the evolution of the dislocation structures is related to the method of deformation loading.

Dislocations exhibit completely different microstructures when different slip modes are activated at the start of shear deformation. Orlova [71] investigated the dislocation microstructures of single crystal copper that was deformed by shear deformation and the shape of the specimen is shown in Figure 7b. The dislocation behaviors were different when the shear stress was applied to different shear planes. The experiment was performed on the shear deformation of double-notched single crystal copper that was acting in the compression direction [110] on different shear planes, which were (1$\bar{1}$1), (1$\bar{1}$3), (1$\bar{1}$0) and (001). The applied shear stress not only activated the crystals that were acting on the chosen shear plane, but also on the other (111)[110] slip systems, leading to a multiple slip activity. As the shear stress was applied to the (1$\bar{1}$1) plane, the slip system (1$\bar{1}$1)[110] had the highest Schmid factor (SF) of 0.98. The observed dislocations moved at lower velocities and failed to escape from the foil. Due to the constraint effects of the shear zones, the dislocations in the other slip system could also be activated. The interactions between the dislocation gliding in the (111)[110] and (111)[0$\bar{1}$1] slip systems could lead to the formation of Lomer–Cottrell junctions, while the tangled dislocation structure was along the [10$\bar{1}$] direction. However, plane the worst slip conditions for the compact systems were when the external force was applied to the (001) due to the Schmid factor being relatively low. The double shear of $\frac{1}{2}$[110] dislocations along the (1$\bar{1}$1) and ($1\bar{1}\bar{1}$) planes became more difficult. The interactions between dislocations that were gliding along the (111)[10$\bar{1}$] and (111)[01$\bar{1}$] systems either eliminated their contributions to the dislocation gliding or cross-slipped to the slip planes of (1$\bar{1}$1) or ($\bar{1}$11). However, when single crystal copper was sheared along

$(1\bar{1}0)[110]$, dislocations with Burgers vectors of a/2[110] cross-slipped to the slip planes of $(1\bar{1}1)$ or $(1\bar{1}\bar{1})$, while dislocations with Burgers vectors of $a/2(1\bar{1}0)$ cross-slipped to the slip planes of (111) or $(11\bar{1})$. Due to the continuous cross-slip of the dislocations, the dislocation structures that were observed by TEM were not very dense and tended to form dislocation cell structures.

In addition, for FCC metallic single crystals that are sheared along $(111)[11\bar{2}]$, the co-planar slip system is activated. As shown in Figure 9, the work hardening rate of single crystal nickel that was sheared along $(111)[\bar{2}11]$ was higher than a specimen that was sheared along $(111)[01\bar{1}]$, but lower than a specimen that was sheared along (100)[010]. However, few researchers have investigated the dislocation structures of co-planar slip systems that are activated under simple shear. As dislocations that have two slip directions that are activated in the same (111) slip plane interact with each other, the dislocation boundary deviates from {111} by more than 10°.

As the crystal rotation mechanism is significantly different under tension and shear, the dislocation structures that are formed during simple shear as are completely different from those that are observed during tension. Lopes et al. [97] investigated the dislocation substructures of an aluminum alloy that was deformed by tension and shear. The dislocation tangles could be observed during the initial stages of tensile deformation without the formation of dislocation cell structures (strain of 6%), while well-defined dislocation cells were formed at strains of about 12%, as shown in Figure 10a,b. However, the dislocation microstructures exhibited straight dislocation walls and the shape of each dislocation cell was identical after simple shear deformation, as shown in Figure 10c,d. A parallelepiped closed cell structure was formed after simple shear deformation because one or two families of the straight dislocation walls were intersecting with each other. The dislocation density inside the cells was different when the aluminum alloy was sheared along different orientations, causing the crystals to exhibit different work hardening rates when deformed along different shear planes and shear directions. Few slip systems were activated during simple shear, which gave rise to the straight dislocation walls and elongated cells.

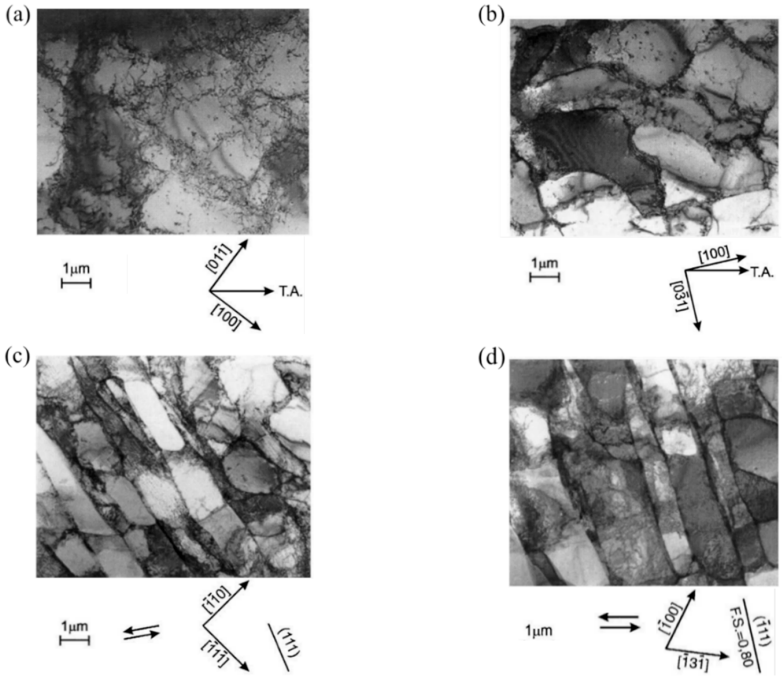

Figure 10. The TEM observations of dislocation tangles after tensile deformation along the [011] orientation when deformed by a strain of (**a**) 0.06 and (**b**) 0.12 and the TEM observations after simple shear deformation at 0.3 shear strain for (**c**) 45° and (**d**) 90° shear [97].

Above all, it would be worthwhile to investigate the crystal rotation mechanism of single crystals that are deformed by simple shear because it could provide an understanding of the contributions of crystal rotation and dislocation interactions to the work hardening of single crystals during shear deformation. The crystal rotation mechanism of single crystals that are deformed by simple shear has not yet been fully elucidated and needs to be investigated further in the future.

4. Concluding Remarks and Prospective Future Research

For an FCC single crystal with a tensile axis that is oriented toward the middle of the orientation triangle, rotation toward the [100]–[111] boundary of the triangle finally becomes stable at [112]; for an FCC single crystal with a tensile axis that is near [111], rotation finally becomes stable at [111]. Crystal rotation is different when it is deformed by tension than when it is formed by simple shear. During simple shear, the slip direction of [110] of an FCC single crystal rotates toward the shear direction, while the crystal is stable when single crystals are sheared along $(1\bar{1}1)[110]$, $(111)[11\bar{2}]$, (001)[110] and $(1\bar{1}2)[110]$.

During tensile testing, the transition from work hardening stage I to stage II is caused by crystal rotation, resulting in an increase in the Schmid factor of the conjugate slip system. The interactions between the dislocations from primary and conjugate slip systems also form a kind of dislocation structure and enhance the work hardening further. Crystal rotation contributes almost nothing to the transition from stage II to stage III; e.g., for the tensile deformation of $[\bar{1}25]$-orientated single crystal aluminum, the parabolic strain hardening behavior that is observed in stage III is caused by caused by the cross-slip of dislocations, which releases the dislocation tangles that were generated in work hardening stage II. The dislocation microstructures from higher strains in work hardening stage III can be classified into three types under tension.

The evolution of dislocation structures is related to the loading modes of the single crystals when they are deformed by simple shear. For FCC single crystals that are directly sheared along $(111)[1\bar{1}0]$, which coincides with one of the 12 slip systems, dislocations may easily glide out of the surface of the slip system with the largest Schmid factor. The dislocations appear as short segments with few tangles and the dislocation density is relatively low because the dislocations from other slip systems hardly activate when the crystals are directly sheared along $(111)[1\bar{1}0]$. In comparison, dislocations easily cross-slip into the other slip plane when they are trapped by obstacles when crystals are sheared along (001)[110]. The dislocation cells and wall structures are formed by the dislocation boundaries that are aligned with the two {101} planes. In contrast, for single crystals that are sheared along $(111)[11\bar{2}]$, the dislocations in the two slip directions that are activated in the same (111) slip plane interact with each other. The work hardening rate is higher than that for single crystals that are sheared along $(1\bar{1}1)[110]$ and the dislocation boundary deviates from {111} by more than 10°.

The general three-stage hardening behavior, including the effects of concurrent crystallographic rotation and the interactions between dislocations from different activated slip systems, is usually clear from tensile testing, which lays the critical foundations for the microstructure, texture and property modeling of polycrystalline metals and alloys in normal strain dominated plastic processes. Over the last few decades, shear strain-dominated severe plastic deformation processing has been extensively investigated to achieve the ultra-refinement of the microstructures and unprecedented properties in metals and alloys. This has raised an urgent need for a fundamental understanding of the path dependency of hardening behavior, including the role of crystallographic rotation in simple shear. It is at this point that a big gap exists between the present knowledge and the perspective achievements of simple shear, which could at least match the achievements of the tensile of single crystals. On top on this, the possibility to elucidate the overall path-dependent hardening behavior of single crystals exists, which covers both normal strain-dominated tensile and shear strain-dominated simple shear.

Author Contributions: Writing—original draft, Z.-W.Z.; writing—review and editing, Z.L.; resources and methodology, Y.L.; supervision and funding acquisition, J.-T.W. All authors have read and agreed to the published version of the manuscript.

Funding: This work was supported by the National Natural Science Foundation of China (grant no.: 52074160).

Institutional Review Board Statement: Not applicable.

Informed Consent Statement: Not applicable.

Data Availability Statement: Not applicable.

Conflicts of Interest: The authors declare no conflict of interest.

References

1. Bellis, J.D.; Bellucci, L.; Bottaro, G.; Labella, L.; Marchetti, F.; Samaritani, S.; Dell'Amico, D.B.; Armelao, L. Single-crystal-to-single-crystal post-synthetic modifications of three-dimensional LOFs (Ln = Gd, Eu): A way to modulate their luminescence and thermometric properties. *Dalton Trans.* **2020**, *49*, 2–26. [CrossRef]
2. Hosono, Y.; Harada, K.; Shimanuki, S.; Saitoh, S.; Yamashita, Y. Crystal growth and mechanical properties of $Pb[(Zn_{1/3}Nb_{2/3})_{0.91}Ti_{0.09}]O_3$ single crystal produced by solution bridgman method. *Jpn. J. Appl. Phys.* **1999**, *38*, 5512–5515. [CrossRef]
3. Fang, Q.; Harada, K.; Shimanuki, S.; Wang, S.J.; Liang, Z.; Jiang, C.Y. Bridgman growth of $LiYF_4$ single crystal in nonvacuum atmosphere. *Chin. Opt. Lett.* **2010**, *8*, 1071–1074. [CrossRef]
4. Mizuno, K.; Yamamoto, S.; Okamoto, H. Ultrahigh-purity aluminium single crystals with a low dislocation density grown by strain-annealing method. *J. Cryst. Growth* **2002**, *237–239*, 367–372. [CrossRef]
5. Ciulik, J.; Taleff, E.M. Dynamic abnormal grain growth: A new method to produce single crystals. *Scr. Mater.* **2009**, *61*, 895. [CrossRef]
6. Mayerhofer, T.G. Symmetric Euler orientation representations for orientational averaging. *Spectrochim. Acta Part A* **2005**, *61*, 2611–2621. [CrossRef]
7. Stricker, M.; Sudmanns, M.; Schulz, K.; Hochrainer, T.; Weygandet, D. Dislocation multiplication in stage II deformation of fcc multi-slip single crystal. *J. Mech. Phys. Solids* **2018**, *119*, 319–333. [CrossRef]
8. Abe, T.; Ono, Y. Numerical study of grain rotation in polycrystalline metal during plastic deformation. *Met. Mater.* **1998**, *4*, 376–379. [CrossRef]
9. Chen, P.; Mao, S.C.; Liu, Y.; Wang, F.; Han, X.D. In-situ EBSD study of the active slip systems and lattice rotation behaviour of surface grains in aluminium alloy during tensile deformation. *Mater. Sci. Eng. A* **2013**, *580*, 114–124. [CrossRef]
10. Han, J.H.; Jee, K.K.; Oh, K.H. Orientation rotation behaviour during in situ tensile deformation of polycrystalline 1050 aluminium alloy. *Int. J. Mech. Sci.* **2003**, *45*, 1613–1623. [CrossRef]
11. Kota, N.; Burak Ozdoganlar, O. A model-based analysis of orthogonal cutting for single-crystal fcc metals including crystallographic anisotropy. *Mach. Sci. Technol.* **2010**, *14*, 102–127. [CrossRef]
12. Seeger, A.; Diehl, J.; Mader, S.; Rebstock, H. Work-hardening and work-softening of face-centred cubic metal crystals. *Philos. Mag.* **1957**, *2*, 323–350. [CrossRef]
13. Mitchell, T.E.; Spitzig, W.A. Three-stage hardening in tantalum single crystals. *Acta Metall.* **1965**, *13*, 1169–1179. [CrossRef]
14. Takeuchi, T. Work hardening of copper single crystals with multiple glide orientations. *Trans. Jpn. Inst. Met.* **1975**, *16*, 629–640. [CrossRef]
15. Yoshida, Y.; Shibano, J.I.; Fukuda, K.I.; Terabayashi, K.; Eguchi, M.; Kajiwara, K.; Shobu, T.; Shiro, A. Crystal rotation and microstructures in an aluminium single-slip system under tensile loading. *Mater. Charact.* **2018**, *146*, 121–126. [CrossRef]
16. Sun, W.C.; Lu, S. A new model for elastic moduli of single-crystal superalloy considering the effect of crystal orientation. *J. Comput. Theor. Nanosci.* **2012**, *12*, 262–266. [CrossRef]
17. Picak, S.; Liu, J.; Hayrettin, C.; Nasim, W.; Karaman, I. Anomalous work hardening behaviour of Fe40Mn40Cr10Co10 high entropy alloy single crystals deformed by twinning and slip. *Acta Mater.* **2019**, *181*, 555–569. [CrossRef]
18. Yu, J.; Dong, C.; Zhang, Q.; Li, B.; Liu, R. Temperature and crystal orientation dependence of dislocation slip and twin nucleation in bilayer Ni/Ni3Al interface. *Comput. Mater. Sci.* **2019**, *162*, 162–170. [CrossRef]
19. Kong, U.; Davepon, B. Microstructure of polycrystalline Ti and its microelectrochemical properties by means of electron-backscattering diffraction. *Electrochim. Acta* **2001**, *47*, 149–160. [CrossRef]
20. Tong, V.; Jones, H.; Mingard, K. Micropillar compression of single crystal tungsten carbide, Part 2: Lattice rotation axis to identify deformation slip mechanisms. *Int. J. Refract. Met. Hard Mater.* **2022**, *103*, 105734. [CrossRef]
21. Han, J.H.; Kim, D.I.; Jee, K.K.; Oh, K.H. In-situ orientation rotation behaviour study during tensile deformation of aluminium single crystal and polycrystal. *Mater. Sci. Forum* **2004**, *449–452*, 593–596. [CrossRef]
22. Luo, Z.; Yoshino, M.; Terano, M.; Yamanaka, A. Texture evolution in single crystal iron static recrystallization through in-situ EBSD observation. *Procedia Manuf.* **2018**, *15*, 1565–1572. [CrossRef]

23. Luis, A.Z.; Alexander, S.; Tomas, O.; Bertin, N.; Barton, N.R.; Freitas, R.; Bulatov, V.V. Atomistic insights in metal hardening. *Nat. Mater.* **2021**, *20*, 315–320.
24. Xu, A.; Wei, T.; Bhattacharyya, D. The effect of strain rate and orientation on He ion irradiated Ni single crystals—An in situ micro-tensile study. *Intern. J. Plast.* **2020**, *126*, 102627. [CrossRef]
25. Reichardt, A.; Ionescu, M.; Davis, J.; Edwards, L.; Harrison, R.P.; Hosemann, P.; Bhattacharyya, D. In situ micro tensile testing of He+2 ion irradiated and implanted single crystal nickel film. *Acta Mater.* **2015**, *100*, 147–154. [CrossRef]
26. Su, J.; Zhu, X. In-situ TEM observation of preferential amorphization in single crystal Si nanowire. *Nanotechnology* **2018**, *29*, 235703. [CrossRef]
27. Namazu, T.; Inoue, S. Characterization of single crystal silicon and electroplated nickel films by uniaxial tensile test with in situ X-ray diffraction measurement. *Fatigue Fract. Eng. Mater. Struct.* **2010**, *30*, 13–20. [CrossRef]
28. Zhang, W.J.; Lu, J.X.; Wang, J.; Sang, L.J.; Ma, J.Y.; Zhang, Y.F.; Zhang, Z. In-situ EBSD study of deformation behaviour of Inconel 740H alloy at high-temperature tensile loading. *J. Alloy. Componds* **2020**, *820*, 153424. [CrossRef]
29. Burger, D.; Dlouhy, A.; Yoshimi, K.; Eggeler, G. On the stress and temperature dependence of low temperature and high stress shear creep in Ni-base single crystal superalloys. *Mater. Sci. Eng. A* **2020**, *795*, 139961. [CrossRef]
30. Mayer, A.E.; Krasnikov, V.S.; Pogorelko, V.V. Dislocation nucleation in Al single crystal at shear parallel to (111) plane: Molecular dynamics simulations and nucleation theory with artificial neural networks. *Int. J. Plast.* **2021**, *139*, 102953. [CrossRef]
31. Lilensten, L.; Couzinie, J.P.; Perriere, L.; Hocini, A.; Keller, C.; Dirras, G.; Guillot, I. Study of a bcc multi-principal element alloy: Tensile and simple shear properties and underlying deformation mechanisms. *Acta Mater.* **2018**, *142*, 131–141. [CrossRef]
32. Zhang, Y.; Wilson, C. Lattice rotation in polycrystalline aggregates and single crystals with one slip system: A numerical and experimental approach. *J. Struct. Geol.* **1997**, *19*, 875–885. [CrossRef]
33. Butler, B.G.; Paramore, J.D.; Ligda, J.P.; Ren, C.; Fang, Z.Z.; Middlemas, S.C.; Hemker, K.J. Mechanisms of deformation and ductility in tungsten—A review. *Int. J. Refract. Met. Hard Mater.* **2018**, *75*, 248–261. [CrossRef]
34. Rao, S.; Woodward, C.; Akdim, B.; Antillon, E.; Parthasarathy, T.A.; EI-Awady, J.A.; Dimiduk, D.M. Large-scale dislocation dynamics simulations of strain hardening of Ni microcrystals under tensile loading. *Acta Mater.* **2019**, *164*, 171–183. [CrossRef]
35. Mark, H.; Polanyi, M.; Schmid, E.; Physik, Z. Vorgänge bei der Dehnung von Zinkkristallen. *Zeitschrift für Physik* **1923**, *12*, 78–110. [CrossRef]
36. Schmid, E.; Boas, W. *Kristallplastizität*; Springer: Berlin, Germany, 1935.
37. Vattre, A.; Devincre, B.; Roos, A. Orientation dependence of plastic deformation in nickel-based single crystal superalloys: Discrete–continuous model simulations. *Acta Mater.* **2010**, *58*, 1938–1951. [CrossRef]
38. Beardmore, P.; Hull, D. Deformation and fracture of tungsten single crystals. *J. Less Common Met.* **1965**, *9*, 168–180. [CrossRef]
39. Argon, A.S.; Maloof, S.R. Plastic deformation of tungsten single crystals at low temperatures. *Acta Metall.* **1966**, *14*, 1449–1462. [CrossRef]
40. Yang, J.R.; Wang, H.; Hu, R.; Zhang, F.; Li, S.M.; Liu, Y.; Luo, X.M. Atomistic simulation of orientation-dependent tension deformation behaviour of single crystal iridium. *Rare Met. Mater. Eng.* **2019**, *48*, 1380–1385.
41. Okada, T.; Fukuoka, T.; Liu, W.Y.; Inoko, F. Rotations involved in tensile deformation and recrystallization in Fe–11Cr–19Ni alloy single crystal. *Isij Int.* **2007**, *40*, 909–913. [CrossRef]
42. Han, J.H.; Kim, D.I.; Jee, K.K.; Oh, K.H. Evolution of crystallographic orientations in an aluminium single crystal during tensile deformation. *Mater. Sci. Eng. A* **2004**, *387–389*, 60–63. [CrossRef]
43. Saai, A.; Tabourot, L.; Depres, C.; Louche, H. A fundamental model of aluminium single crystals behaviour with physical description of kinematic work hardening. *Mater. Sci. Forum* **2007**, *550*, 577–582. [CrossRef]
44. Paik, S.; Naveen Kumar, N.; Dutta, B.K.; Durgaprasad, P.V.; Tewari, R. Deformation of copper single crystals: Comparison of experimental results with crystal plasticity simulations. *Mater. Today Commun.* **2020**, *24*, 100997. [CrossRef]
45. Kim, K.H.; Koo, Y.M. In-situ X-ray diffraction study of single-slip-conditioned copper single crystals during uniaxial deformations. *Philos. Mag. A* **2001**, *81*, 479–488. [CrossRef]
46. Hosford, W.F. *The Mechanics of Crystals and Textured Polycrystals*; Oxford University Press: New York, NY, USA, 1993.
47. Xu, A.; Saleh, M.; Davis, J.; Edwards, L.; Bhattacharyya, D. In-situ micro-tensile investigation of strain rate response along and directions in single crystal nickel. *Int. J. Plast.* **2018**, *106*, 129–144. [CrossRef]
48. Cottrell, A.H. Commentary. A brief view of work hardening. *Dislocations Solids* **2002**, *11*, vii–xvii.
49. Ungar, T.; Stoica, A.D.; Tichy, G.; Wang, X.L. Orientation-dependent evolution of the dislocation density in grain populations with different crystallographic orientations relative to the tensile axis in a polycrystalline aggregate of stainless steel. *Acta Mater.* **2014**, *66*, 251–261. [CrossRef]
50. Zheng, W.; Wangyue, Y.; Zuqing, S. Orientation dependency of shear stress-strain curves in B2-ordered Fe3Al single crystals deformed in tension at room temperature. *Sci. China* **2002**, *45*, 314–320. [CrossRef]
51. Tang, M.; Marian, J. Temperature and high strain rate dependence of tensile deformation behaviour in single-crystal iron from dislocation dynamics simulations. *Acta Mater.* **2014**, *70*, 123–129. [CrossRef]
52. Song, W.; Wang, X.G.; Li, J.G.; Meng, J.; Sun, X.F. Effect of Ru on tensile behaviour and deformation mechanism of a nickel-based single crystal superalloy. *Mater. Sci. Eng. A* **2021**, *802*, 140430. [CrossRef]
53. Winther, G.; Huang, X. Dislocation structures. Part 2. Slip system dependence. *Philos. Mag.* **2007**, *87*, 5215–5235. [CrossRef]

54. Srivastava, K.; Weygand, D.; Caillard, D.; Gumbsch, P. Repulsion leads to coupled dislocation motion and extended work hardening in bcc metals. *Nat. Commun.* **2020**, *11*, 5098. [CrossRef] [PubMed]
55. Mishra, A.; Alankar, A. Revisiting dislocation reactions and their role in uniaxial deformation of copper single crystal micro-pillars. *Model. Simul. Mater. Sci. Eng.* **2019**, *27*, 005010. [CrossRef]
56. Devincre, B.; Kubin, L.P. Simulations of forest interactions and strain hardening in FCC crystals. *Model. Simul. Mater. Sci. Eng.* **1994**, *2*, 559. [CrossRef]
57. Jiao, B.; Zhao, Q.; Zhao, Y.; Li, L.; Li, J. The relationship between slip behaviour and dislocation arrangement for large-size Mo-3Nb single crystal at room temperature. *J. Mater. Sci. Technol.* **2021**, *92*, 208–213. [CrossRef]
58. Hansen, N.; Huang, X.; Winther, G. Effect of grain boundaries and grain orientation on structure and properties. *Metall. Mater. Trans.* **2011**, *42*, 613–625. [CrossRef]
59. Rahmati, S.; Veiga, R.; Jodoin, B.; Zuiga, A. Crystal orientation and grain boundary effects on plastic deformation of FCC particles under high velocity impacts. *Materialia* **2021**, *15*, 101004. [CrossRef]
60. Lim, H.; Noell, P.J.; Carroll, J.D. Crystallographic orientation dependent fracture behaviour in tantalum single crystals. *Scr. Mater.* **2021**, *191*, 76–80. [CrossRef]
61. Oh, S.H.; Legros, M.; Daniel, K.; Dehm, G. In situ observation of dislocation nucleation and escape in a sub-micrometer aluminium single crystal. *Nat. Mater.* **2009**, *8*, 95–100. [CrossRef]
62. Huang, X.; Winther, G. Dislocation structures. Part, I. Grain orientation dependence. *Philos. Mag.* **2007**, *87*, 5189–5214. [CrossRef]
63. Irwin, G.J.; Guiu, F.; Pratt, P.L. The influence of orientation on slip and strain hardening of molybdenum single crystal. *Phys. Stat. Sol.* **1974**, *22*, 685–698. [CrossRef]
64. Li, Y.; Chatterjee, S.; Martinez, E.; Ghoniem, N.; Po, G. On the cross-slip of screw dislocations in zirconium. *Acta Mater.* **2021**, *208*, 116764. [CrossRef]
65. Landau, P.; Shneck, R.; Makov, G.; Venkert, A. In-situ TEM study of dislocation patterning during deformation in single crystal. *J. Phys. Conf. Ser.* **2010**, *241*, 012060. [CrossRef]
66. Burton, B. The dislocation network theory of creep. *Philos. Mag. A* **1982**, *45*, 657–675. [CrossRef]
67. Miyauchi, K. *Rotation Problems in Simple Shear Deformation*; Springer: Dordrecht, The Netherlands, 1991.
68. G'Sell, C.; Gopez, A.J. Plastic banding in glassy polycarbonate under plane simple shear. *J. Mater. Sci.* **1985**, *20*, 3462–3478. [CrossRef]
69. Rauch, E.; G'Sell, C. Flow localization induced by a change in strain path in mild steel. *Mater. Sci. Eng. A* **1989**, *111*, 71–80. [CrossRef]
70. Mayr, C.; Eggeler, G.; Webster, G.A.; Peter, G. Double shear creep testing of superalloy single crystals at temperature above 1000 °C. *Mater. Sci. Eng. A* **1995**, *199*, 121–130. [CrossRef]
71. Orlová, A. Dislocation structures on the plane of shear in compressed double-notch copper single crystal specimens. *Mater. Sci. Eng. A* **1999**, *260*, 94–100. [CrossRef]
72. Cao, L.; Thome, P.; Jácome, L.A.; Somsen, C.; Cailletaud, G.; Eggeler, G. On the influence of crystallography on creep of circular notched single crystal superalloy specimens. *Mater. Sci. Eng.* **2020**, *782*, 139255. [CrossRef]
73. An, Y.; Vegter, H.; Heijne, J. Development of simple shear test for the measurement of work hardening. *J. Mater. Processing Technol.* **2009**, *209*, 4248–4254. [CrossRef]
74. Peirs, J.; Verleysen, P.; Paepegem, W.V.; Degrieck, J. Determining the stress-strain behaviour at large strains from high strain rate tensile and shear experiments. *Int. J. Impact Eng.* **2011**, *38*, 406–415. [CrossRef]
75. Pettersson, K.B. The Inclined Double Notch Shear Test for Determination of Interlaminar Shear Properties of Composite Laminates. Ph.D. Thesis, KTH Royal Institute of Technology, Stockholm, Sweden, 2005.
76. Petterson, K.B.; Neumeister, J.M.; Strandberg, M. V-notched shear specimens for the inclined double notch shear test. *J. Test. Eval.* **2007**, *35*, 85–94.
77. Katayama, S.; Miyamoto, H.; Vinogradov, A.; Hashimoto, S. Influence of a slip plane orientation with respect to the shear plane of ECAP on microstructure of copper single crystal subject to one pressing at room temperature. *Mater. Sci. Forum* **2008**, *584–586*, 387–392. [CrossRef]
78. Guo, T.; Wei, S.; Wang, C.; Li, Q.; Jia, Z. Texture evolution and strengthening mechanism of single crystal copper during ECAP. *Mater. Sci. Eng.* **2019**, *759*, 97–104. [CrossRef]
79. Li, S.; Beyerlein, I.J.; Bourke, M.A. Texture formation during equal channel angular extrusion of FCC and bcc materials: Comparison with simple shear. *Mater. Sci. Eng. A* **2005**, *394*, 66–77. [CrossRef]
80. Khlebnikova, Y.V.; Egorova, L.Y.; Pilyugin, V.P.; Suaridze, T.R.; Patselov, A.M. Evolution of the structure of an α-titanium single crystal during high-pressure torsion. *Tech. Phys.* **2015**, *60*, 1005–1013. [CrossRef]
81. Gravell, J.D.; Ryu, I. Latent hardening/softening behaviour in tension and torsion combined loadings of single crystal FCC micropillars. *Acta Mater.* **2020**, *190*, 58–69. [CrossRef]
82. Wang, H.; Lu, C.; Wang, R. A crystal plasticity FEM study on macro- and micro-subdivision of an aluminium single crystal after multi-pass unidirectional rolling, reverse rolling and accumulative roll-bonding. *Int. J. Adv. Manuf. Technol.* **2020**, *111*, 37–51. [CrossRef]
83. Wang, H.; Lu, C.; Tieu, K.; Liu, Y. A crystal plasticity FE study of macro- and micro-subdivision in aluminium single crystals {001} multi-pass rolled to a high reduction. *J. Mater. Sci. Technol.* **2020**, *76*, 231–246. [CrossRef]

84. Tome, C.; Canova, G.R.; Kocks, U.F.; Christodoulou, N.; Jonas, J.J. The relation between macroscopic and microscopic strain hardening in F.C.C. polycrystals. *Acta Metall.* **1984**, *32*, 1637–1653. [CrossRef]
85. Eggeler, G.; Wieczorek, N.; Fox, S.; Berglund, S.; Burger, D.; Dlouhy, A.; Wollgramm, P.; Neuking, K.; Schreuer, J.; Jacome, L.A.; et al. On shear testing of single crystal Ni-Base superalloys. *Metall. Mater. Trans. A* **2018**, *49A*, 3951–3962. [CrossRef]
86. Hayakawa, M.; Nakayama, E.; Okamura, K.; Yamamoto, M.; Shizawa, K. Development of micro-shear fatigue test and its application to single crystal of pure iron. *Procedia Eng.* **2016**, *160*, 167–174. [CrossRef]
87. Paul, H.; Driver, J.; Maurice, C.; Jasieński, Z. Shear band microtexture formation in twinned face centred cubic single crystals. *Mater. Sci. Eng. A* **2003**, *359*, 178–191. [CrossRef]
88. Heyer, J.K.; Brinckmann, S.; Pfetzing-Micklich, J.; Eggeler, G. Micro-shear deformation of gold single crystals. *Acta Mater.* **2014**, *62*, 225–238. [CrossRef]
89. Laplanche, G.; Wieczorek, N.; Fox, F.; Berglund, S.; Pfetzing-Micklich, J.; Kishida, K.; Inui, H.; Eggeler, G. On the influence of crystallography and dendritic microstructure on micro shear behaviour of single crystal Ni-based superalloys. *Acta Mater.* **2018**, *160*, 173–184. [CrossRef]
90. Seok, M.Y.; Gopalan, H.; Nandy, S.; Zaefferer, S.; Raabe, D.; Kirchlechner, C.; Dehm, G. Microscale plastic anisotropy of basal and pyramidal I slip in pure magnesium tested in shear. *Materialia* **2020**, *14*, 100932. [CrossRef]
91. Wieczorek, N.; Laplanche, G.; Heyer, J.K.; Parsa, A.B.; Pfetzing-Micklich, J.; Eggeler, G. Assessment of strain hardening in copper single crystals using in situ SEM micro-shear experiments. *Acta Mater.* **2016**, *113*, 320–334. [CrossRef]
92. Hiroshi, F.; Shiro, K. Role of conjugate slip in deformation of Cu-10at%Al single crystals. *J. Phys. Soc. Jpn.* **1983**, *52*, 157–167.
93. Al-Fadhalah, K.J.; Alhajeri, S.N.; Almazrouee, A.I.; Langdon, T.G. Microstructure and microtexture in pure copper processed by high-pressure torsion. *J. Mater. Sci.* **2013**, *48*, 4563–4572. [CrossRef]
94. Franciosi, P.; Berveiller, M.; Zaoui, A. Latent hardening in copper and aluminium. *Acta Metall.* **1980**, *28*, 273–283. [CrossRef]
95. Liu, Q.; Wert, J.; Hansen, N. Location-dependent lattice rotation and shear strain in rolled aluminium single crystals of cube and Goss orientations. *Acta Mater.* **2000**, *48*, 4267–4279. [CrossRef]
96. Takayama, Y.; Xu, Y.; Yoshida, T.; Tanaka, H.; Onuki, Y.; Satoet, S. Texture evolutions in aluminium and Al-3%Mg alloy subjected to shear deformation and subsequent annealing. *IOP Conf. Ser. Mater. Sci. Eng.* **2021**, *1121*, 012017. [CrossRef]
97. Lopes, A.B.; Barlat, F.; Gracio, J.J.; Ferreira, J.F.; Rauch, E.F. Effect of texture and microstructure on strain hardening anisotropy for aluminium deformed in uniaxial tension and simple shear. *Int. J. Plast.* **2003**, *19*, 1–12. [CrossRef]